BIOCHEMISTRY
including biophysical chemistry & molecular biology
Article

Biochemistry **2010,** *49,* 7615–7624 7615
DOI: 10.1021/bi100745j

Salt-Induced Modulation of the Pathway of Amyloid Fibril Formation by the Mouse Prion Protein[†]

Shweta Jain and Jayant B. Udgaonkar*

National Centre for Biological Sciences, Tata Institute of Fundamental Research, Bangalore 560065, India

Received May 11, 2010; Revised Manuscript Received July 12, 2010

ABSTRACT: To investigate how the heterogeneity inherent in the formation of worm-like amyloid fibrils by the mouse prion protein is modulated by a change in aggregation conditions, as well as to determine how heterogeneity in reaction leads to heterogeneity in structure, the amyloid fibril formation reaction of the protein at low pH was studied in the presence of various salts. It is shown that β-rich oligomers of different sizes and structures are formed at low and high NaCl concentrations, as determined by Fourier transfer infrared (FTIR) spectroscopy and dynamic light scattering (DLS). The worm-like fibrils formed from the β-rich oligomers at low and high NaCl concentrations also differ in their internal structure, as determined by FTIR measurements. The apparent rate constant for the formation of the worm-like amyloid fibrils shows a very steep sigmoidal dependence on NaCl concentration, suggesting that the effect occurs because of the binding of many ions. The effect of salt in modulating the kinetics of worm-like fibril formation occurs at ionic strengths below 200 mM, over different concentration ranges for different salts, and is shown to depend not only on the ionic strength but also on the nature of the anion. The ability of different anions to promote worm-like fibril formation does not follow the Hofmeister series but instead follows the electroselectivity series for anion binding. Hence, it appears that the effect of salt is because of the linkage of the aggregation reaction to anion binding to the protein. A comparison of the apparent rate constants measured from the changes in thioflavin T fluorescence, circular dichroism, and DLS, which occur during worm-like fibril formation, suggests that conformational conversion follows fibril elongation at low NaCl concentration and follows fibril formation at high NaCl concentration.

Prion diseases are a group of fatal neurodegenerative diseases that appear to originate from the misfolding of normal cellular prion protein, PrP^C, into an alternative disease-related conformation, PrP^{Sc} (*1*, *2*). PrP^C exists as a GPI-anchored, monomeric, protease-sensitive conformation and is rich in α-helix. Although its structure is not known, PrP^{Sc} is known to be oligomeric, protease-resistant, and rich in β-structure (*2*−*5*). It is now believed that PrP^{Sc} is formed by amyloidogenic aggregation, via autocatalytic conversion, of PrP^C (*6*−*11*). Hence, understanding the process of amyloid formation by the prion protein becomes imperative.

Bacterially expressed recombinant PrP is usually used to study the aggregation of the prion protein. In the recombinant prion protein, unlike in the original mammalian protein, the disulfide bond between C179 and C214 is retained, but glycosylation at N181 and N193 and the GPI anchor at the C-terminus are absent. A recent report has suggested that recombinant mouse prion protein can be converted into infectious prion isoforms in the presence of specific lipids and RNA (*12*). The recombinant prion protein therefore becomes a very useful model for studying the molecular mechanism of the conversion of PrP^C to PrP^{Sc}.

[†]This work was funded by the Tata Institute of Fundamental Research and by the Department of Biotechnology, Government of India. J.B.U. is a recipient of a J. C. Bose National Fellowship from the Government of India.

*To whom correspondence should be addressed: National Centre for Biological Sciences, Tata Institute of Fundamental Research, Bangalore 560065, India. Telephone: 91-80-23666150. Fax: 91-80-23636462. E-mail: jayant@ncbs.res.in.

The prion protein has two domains, an unstructured N-terminal domain (residues 23−120) and a folded C-terminal domain (residues 121−231). In most studies so far, a truncated form of the prion protein (either residues 90−231 or residues 120−231) has been used, because it has been shown that residues 23−90 are not essential for prion transmission (*3*, *13*). The N-terminal region may, however, be important in prion pathogenesis and for defining prion strains. Bivalent metal ions, such as Cu^{2+}, bind to the N-terminal region of the protein encompassing residues 23−90 and have been shown to induce partial structure in this region (*14*). Furthermore, Cu^{2+} ions have been shown to modulate pathogenesis in prion diseases (*15*−*18*).

The aggregation reactions of proteins appear to proceed from aggregation-competent partially structured conformations that are either stable or kinetically trapped (*19*−*22*). Such partially unfolded intermediates can be populated upon mutation, upon a change in the solvent conditions, as well as upon interaction of the protein with ligands (*23*−*28*). It is possible that different subpopulations of the aggregation-competent intermediates accumulate under different aggregation conditions. One important variable in this context is salt concentration, and salts have been shown to affect protein aggregation reactions in diverse ways. It was seen in the case of α-synuclein and the yeast prion protein Sup35 that salts affect the aggregation reaction through the Hofmeister effect (*29*, *30*). On the other hand, in the case of β_2-microglobulin and glucagon, specific anion binding was shown to play an important role in the aggregation process (*31*, *32*). In the case of amyloid-β, both

Published on Web 07/14/2010

the Hofmeister effect and specific anion binding appear to be important (*33*).

One of the interesting features of the prion proteins, seen in both mammalian and yeast proteins, is the phenomenon of strain diversity, in which a prion protein can adopt a number of distinct conformations, which may display different phenotypes differing in their incubation periods, in the areas of the brain they affect, and in their pathologies (*4*, *5*, *11*). In vitro studies have shown that prion protein aggregates are extremely heterogeneous; the same protein can assemble into many different amyloid structures (*34*−*36*). Understanding the structural heterogeneity seen in prion protein aggregates has now become an important goal of prion aggregation studies. In this context, determining how a change in aggregation conditions, effected by the presence of different salts, affects the kinetics of prion protein aggregation is important, because it might provide an insight into the mechanistic basis of the structural heterogeneity inherent in prion protein aggregation and would therefore help in the understanding of the phenomenon of prion strain diversity. Furthermore, understanding the molecular mechanisms by which salts affect the aggregation of proteins might provide ways of modulating the reaction.

The α-rich monomeric form of the mouse prion protein (moPrP)[1] has been shown to exist in equilibrium with β-rich oligomers (*37*). The equilibrium favors the α-rich monomer at pH 7 and the β-rich oligomer at pH 2. The α-rich monomers can aggregate to long straight amyloid fibrils (*38*). The β-rich oligomers transform into worm-like fibrils in multiple steps in 150 mM NaCl at pH 2: β-sheet conformational conversion occurs concurrently with fibril elongation, and the elongated fibrils then associate laterally to form the mature worm-like fibrils (*37*).

In this study, the effects of different salts on the formation of worm-like fibrils by the moPrP have been investigated using multiple structural probes. It is seen that NaCl enhances the rate of worm-like fibril formation in a concentration-dependent manner. Interestingly, the β-rich oligomers formed at low and high NaCl concentrations are structurally distinct and follow different pathways for their transformation into worm-like fibrils. In 120 mM NaCl, β-sheet conformational conversion appears to follow aggregate elongation (growth), while in 200 mM NaCl, it appears to precede aggregate elongation. The worm-like fibrils formed on the alternative pathways are seen to differ in their internal structures. The effects of salts on the formation of the worm-like fibrils cannot be explained either by Debye−Huckel charge screening or by the Hofmeister effect. Rather, it appears that salts affect the kinetics of this process by directly binding to the protein.

EXPERIMENTAL PROCEDURES

Protein Expression and Purification. The expression and purification of wild-type (wt) moPrP have been described previously (*37*). The purity of the protein was confirmed by SDS−PAGE and ESI-MS. The mass of the protein was the expected 23236 Da, when determined by mass spectrometry using an ESI-QTOF mass spectrometer from Waters. The protein was stored in 10 mM sodium acetate buffer (pH 4) at −80 °C, as described previously.

[1]Abbreviations: moPrP, mouse prion protein; ThT, thioflavin T; CD, circular dichroism; θ_{216}, ellipticity at 216 nm; DLS, dynamic light scattering; R_H, hydrodynamic radius; SI, scattering intensity; FTIR, Fourier transform infrared; AFM, atomic force microscopy.

Buffers, Solutions, and Experimental Conditions. All reagents used for the experiments were of the highest purity grade available from Sigma. The protein in 10 mM sodium acetate buffer (pH 4) was diluted 2-fold with 2× aggregation buffer, so that the protein was finally in 50 mM glycine buffer containing the desired concentration of NaCl, or any other salt, at pH 2. The final protein concentration used for most of the experiments was 25 μM, except for the FTIR studies, as described.

Aggregation Studies. The aggregation process was monitored by measurement of ThT fluorescence, ellipticity at 216 nm (θ_{216}), and dynamic light scattering (DLS). For all the measurements, the protein was first incubated for 1 h in aggregation buffer at 25 °C. After incubation for 1 h, the protein was transferred into a tube in the heating block, preset at 50 ± 0.5 °C. The same heating block was used for all the experiments to reduce variability. The temperature jump of the protein solution was complete within 4 min of incubation in the heating block. At different time points of aggregation, aliquots of the protein sample were withdrawn for analysis by ThT fluorescence, θ_{216}, and DLS. All the sample aliquots withdrawn for analysis by the different probes were treated in manners as similar as possible.

It was important to show that prolonged incubation of the protein at pH 2 in 120 mM NaCl at 50 °C did not result in hydrolysis of the polypeptide chain. A sample of protein that had been incubated for 19 h at pH 2 and 50 °C was therefore subjected to SDS−PAGE. No significant hydrolysis of the protein was observed (data not shown).

Thioflavin T Fluorescence Assay. For the assay, final concentrations of 2 μM protein and 20 μM ThT were used. A calculated amount of protein was withdrawn from the sample and added to the ThT-containing assay solution (50 mM Tris at pH 8). ThT fluorescence was measured using a Fluoromax-3 spectrofluorimeter (Jobin Yvon). The experimental settings used were as follows: excitation wavelength, 440 nm; emission wavelength, 482 nm; excitation bandwidth, 1 nm; and emission bandwidth, 10 nm. Measurements were taken within 30 s of the addition of the protein to the assay solution.

Circular Dichroism Measurements. A Jasco J-720 spectropolarimeter was used for the far-UV CD measurements. A cuvette with a path length of 1 mm was used. For the acquisition of spectra, the protein was diluted to 12.5 μM just before the measurement. Spectra were recorded in the wavelength range of 200−250 nm. The following instrument settings were used: step resolution, 1 nm; scan speed, 100 nm/min; and bandwidth, 1 nm. Each spectrum was averaged for over 30 scans. For the kinetic studies, the ellipticity at 216 nm was monitored at regular time intervals.

Dynamic Light Scattering Measurements. A DynaPro-99 unit (Wyatt) was used for the DLS measurements. All the buffers and the protein solutions at pH 4 were filtered using 0.02 μm filters to remove dust particles. Filtered buffers and the protein solution at pH 4 were centrifuged at 10000 rpm for 10 min. All the tubes and tips used for the experiment were rinsed three times with 0.02 μm filtered water before use. The pH jump, from 4 to 2, was given with the 0.02 μm filtered buffer. The protein sample was incubated for 1 h at 25 °C before the temperature jump to 50 °C. After the temperature jump, aliquots of the protein sample were withdrawn for the measurement at regular time intervals. The protein sample was cooled to 25 °C and then placed in a 45 μL cuvette. The cuvette was placed in the sample chamber

maintained at 25 °C for the measurement. The following experimental settings were used: acquisition time, 5 s; signal-to-noise threshold, 2.5; and sensitivity, 70%. The sample was illuminated with a laser of wavelength of 829.4 nm, and the scattering intensity at 90° and its autocorrelation function were measured simultaneously. Fluctuations of more than 15% in the scattering intensity were excluded from analysis. DynaLS (Wyatt) was used to resolve the accepted acquisitions into well-defined Gaussian distributions of hydrodynamic radii. The viscosities of the solutions were determined from refractive index measurements. The total light scattering intensity (counts per second) was determined from the cumulants analysis as the mean of all accepted acquisitions.

Size Exclusion Chromatography. The hydrodynamic properties of moPrP were studied using gel filtration on a Waters Protein Pak 300-SW column using an Akta (GE) chromatography system. The fractionation range of the 15.1 mL column was 10−300 kDa, and the void volume was determined to be 6.2 mL. Each protein sample was equilibrated in 50 mM glycine buffer, with the desired amount of NaCl at pH 2 for 1 h prior to the acquisition of the chromatogram. Before injection of 50 μL of the protein solution, the column was equilibrated with 4 column volumes of the same buffer. In the case of the native protein, the column was equilibrated with 100 mM sodium acetate buffer (pH 4). A flow rate of 0.72 mL/min was used.

Fourier Transform Infrared Spectroscopy Measurement. FTIR measurements were taken using a Thermo Nicholet-6700 FTIR spectrometer (Thermo Scientific) equipped with a liquid nitrogen-cooled MCT detector. Buffers (see above) made in H_2O were used. The spectrometer was purged with ultrapure nitrogen gas. Oligomers and worm-like fibrils were formed by 25 μM protein at pH 2, in the presence of 120 and 200 mM NaCl. The solutions were concentrated ~20-fold for the oligomers formed in 120 or in 200 mM NaCl, as well as for the worm-like fibrils formed in 120 mM NaCl. Worm-like fibrils formed in 200 mM NaCl could not be concentrated more than ~8-fold, because of protein precipitation. Centricons (Millipore Corp.) with a 10 kDa cutoff were used for concentrating the oligomer and fibril solutions. The concentrated samples were applied to a diamond crystal, and spectra were recorded in the attenuated total reflectance (ATR) mode at a resolution of 4 cm^{-1}. Before each of the acquisitions of sample data, the buffer spectrum was recorded under identical conditions and was used as the blank. For each sample, 256 scans were averaged.

Atomic Force Microscopy. For the AFM studies, 25 μM protein in 50 mM glycine buffer (pH 2) containing the desired amount of NaCl or any other salt was heated to 50 °C. An aliquot of the sample was withdrawn and diluted to 0.5 μM in aggregation buffer. The diluted sample was applied on to a freshly cleaved mica sheet and incubated for 1 min. The mica surface was then rinsed three times with filtered water at pH 2 and dried under vacuum for 45 min before it was scanned. The AFM images were obtained using a PicoPlus AFM instrument (Molecular Imaging Inc.) operating in the noncontact mode, as described previously (*37*). The diameters of aggregates were determined from the *Z*-heights in AFM images, using the profile option of WSXM (*39*). For each salt, 25 individual protofibrils were monitored. The height of each individual protofibril was determined as the mean of the heights determined along its length. The lengths of worm-like amyloid fibrils were also calculated using the profile option of WSXM (*39*).

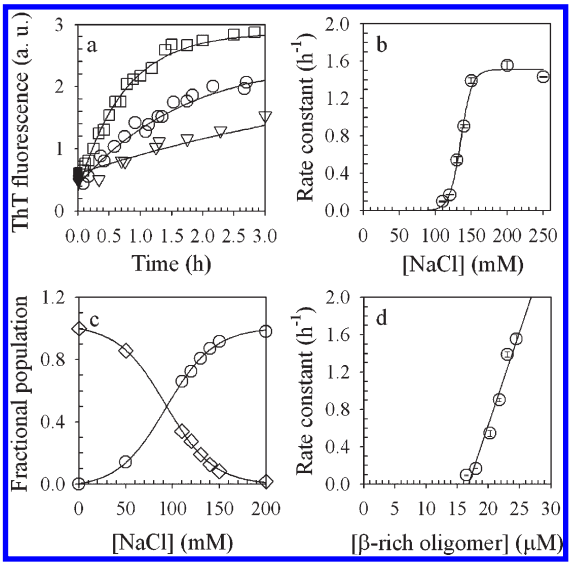

FIGURE 1: Effect of NaCl on the kinetics of amyloid fibril formation and β-rich oligomer formation by 25 μM moPrP at pH 2 and 50 °C. (a) ThT fluorescence-monitored kinetic traces of amyloid fibril formation by 25 μM protein in the presence 120 (▽), 130 (○), 150 mM NaCl (□) at pH 2 and 50 °C. (b) Dependence of the apparent rate constant of amyloid fibril formation on NaCl concentration. The apparent rate constants were determined from single-exponential fits of the kinetic traces. The error bars represent the spreads in the values obtained from two independent experiments. (c) Fractional amount of β-rich oligomer (○) and monomer (◇) at different NaCl concentrations at pH 2. The fractional amount of each protein form was calculated after integration of the areas under the respective peaks in the size exclusion chromatogram of the protein at each salt concentration. The solid lines have been drawn by inspection only. (d) Dependence of the apparent rate constant of worm-like amyloid fibril formation on the amount of β-rich oligomer. The apparent rate constants were determined from single-exponential fits of the kinetic traces. The error bars represent the spreads in the values obtained from two independent experiments. The concentration of the β-rich oligomer at each salt concentration was determined by multiplication of the fraction of protein present as the β-rich oligomer (c) by the total monomeric protein concentration (25 μM). The straight line through the data is a least-squares fit.

RESULTS

Effect of NaCl on the Kinetics of Fibril Formation from β-Rich Oligomers. The oligomers formed in the presence of NaCl transform into worm-like fibrils in a process that becomes faster at higher temperatures (*37*). Figure 1a shows the thioflavin T (ThT) fluorescence-monitored kinetics of the formation of worm-like amyloid fibrils from β-rich oligomers at NaCl concentrations of 120, 130, and 150 mM. The kinetics at < 110 mM NaCl was too slow to be measured. At each NaCl concentration, no lag phase is apparent and the kinetics appears to be monophasic. At each NaCl concentration, kinetic traces extrapolate, at time zero, to the signal obtained for β-rich oligomers. The observed rate constant is seen to increase with an increase in NaCl concentration. When the same reaction was conducted in the presence of 150 mM KCl, the kinetics was found to be identical to that seen in the presence of 150 mM NaCl (data not shown). This suggests that the salt effect is primarily an anion-induced effect.

In Figure 1b, the apparent rate constant of worm-like fibril formation, determined from single-exponential fits to the kinetic traces obtained at different NaCl concentrations, is plotted versus NaCl concentration. The high reproducibility of experiments is evident from the small errors in the measurements of the apparent

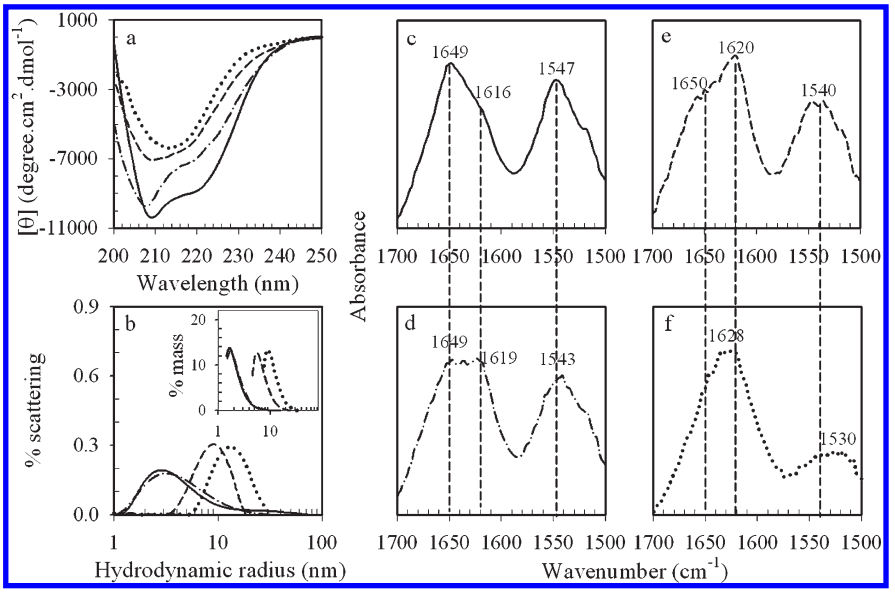

FIGURE 2: Characterization of β-rich oligomers formed at different salt concentrations. (a) Far-UV CD spectra. (b) DLS distributions. In panels a and b, the solid lines, dashed−dotted lines, dashed lines, and dotted lines represent data for the native protein at pH 4, the protein in the absence of NaCl at pH 2, the protein in 120 mM NaCl at pH 2, and the protein in 200 mM NaCl at pH 2, respectively. The protein concentration was 25 μM in all cases. (c) FTIR spectrum of native protein at pH 4 acquired at 3 mM protein. (d) FTIR spectrum of protein at pH 2 in the absence of any salt, where 70% of the protein is present as oligomer and 30% protein is monomeric. (e) Spectrum of the oligomer formed by 25 μM protein after 1 h in 120 mM NaCl at pH 2 and 25 °C. (f) Spectrum of the oligomer formed by 25 μM protein after 1 h in 200 mM NaCl at pH 2 and 25 °C. For acquisition of the data in panels e and f, the oligomers were first concentrated to 500 μM, where > 98% of the protein is present as oligomer.

rate constants. The apparent rate constant is seen to increase sharply in a sigmoidal manner with an increase in NaCl concentration, over a very narrow concentration range (~100−150 mM), which suggests that NaCl may affect the kinetics of worm-like fibril formation by a direct interaction with the protein.

In a previous study, it was shown that the observed rate constant of amyloid fibril formation is directly proportional to the amount of β-rich oligomer formed at pH 2, and not to the amount of monomer present (*37*). In that study, the relative population of β-rich oligomer was varied by changing the protein concentration at a fixed NaCl concentration and estimating the amount of β-rich oligomer by size exclusion chromatography. The observation that the observed rate constant of fibril formation varies with NaCl concentration suggested that the effect of increasing the salt concentration might be to increase the amount of β-rich oligomer present.

Figure 1c shows that the relative amounts of β-rich oligomer and monomer present formed by 25 μM protein, estimated by size exclusion chromatography (*37*), do indeed change in a continuous sigmoidal manner, with a change in NaCl concentration. Figure 1d shows that the observed rate constant of fibril formation has a linear dependence on the concentration of β-rich oligomer, when the latter was varied by varying the NaCl concentration in the range of 110−200 mM for a fixed (25 μM) protein concentration. Below 110 mM, the aggregation kinetics is too slow to be measured, even though a substantial fraction of the protein is found to be β-rich oligomer (Figure 1c). The discontinuity seen at ~110 mM NaCl (Figure 1d) in the dependence of the observed rate constant on β-rich oligomer concentration suggests that the structure of the β-rich oligomer changes at this salt concentration. The dependence of the observed rate constant on β-rich oligomer concentration, when the latter is varied in the range of 15−25 μM via variation of the NaCl concentration in the range of 110−200 mM, is much stronger than when the β-rich oligomer concentration is varied in the same range via variation of the protein concentration at a fixed (150 mM) NaCl concentration (*37*). This result suggests that an increase in the NaCl concentration from 110 to 200 mM changes not only the amount of β-rich oligomer formed but also its structure.

Spectroscopic Characterization of β-Rich Oligomers Formed at Low and High NaCl Concentrations. The far-UV CD spectrum of the protein at pH 2 in the absence of added NaCl shows that the protein has lost some of the secondary structure present in the native protein at pH 4, but that it remains rich in α-helix (Figure 2a). Upon addition of NaCl at pH 2, the protein adopts an alternative β-rich conformation, which becomes more distinctive with an increase in salt concentration (Figure 2a). DLS measurement of the R_H distribution of the protein at pH 2 shows that the distribution is similar to that of the native protein at pH 4 (Figure 2b), indicating that the protein at pH 2 in the absence of added NaCl is predominantly monomeric. Upon addition of NaCl, the R_H distributions show that the protein oligomerizes (Figure 2b) and that the β-rich oligomer is larger at a higher NaCl concentration. The mean values of R_H are ~11 and 17 nm at 120 and 200 mM NaCl, respectively. The far-UV CD and DLS data were collected using 25 μM protein. In 120 mM NaCl, ~72 and ~28% of the protein are present as oligomer and monomer, respectively. In 200 mM NaCl, ~98 and < 2% of the protein are present as oligomer and monomer, respectively (Figure 1c). The 28% monomeric protein present in 120 mM NaCl is not seen in the DLS distribution presumably because its scattering is overwhelmed by that of the 72% oligomer present.

Panels c−f of Figure 2 show the Fourier transform infrared (FTIR) spectra of the protein under different conditions. In a FTIR spectrum, a peak in the region of 1613−1643 cm^{-1} corresponds to β-sheet-rich structures, and a peak at ~1650 cm^{-1} represents α-helix and/or random coil structures (*40*−*42*). Consistent with the known NMR structure of the native prion protein (*43*, *44*), the FTIR spectrum of monomeric moPrP at pH 4 shows a peak at ~1649 cm^{-1} with a shoulder at ~1616 cm^{-1}. The FTIR spectrum was recorded at a protein concentration of 3 mM at pH 4; size exclusion chromatography shows that at this

protein concentration, at which the FTIR spectrum was recorded, the protein remains monomeric (data not shown).

At pH 2 in the absence of NaCl, the protein remains monomeric at a low protein concentration (Figure 2b), but 70% of the protein molecules were seen by size exclusion chromatography (data not shown) to assemble into oligomers at a concentration of 1.5 mM which was necessary for measurement of the FTIR spectrum. The presence of peaks at ~1619 and ~1649 cm^{-1} in the FTIR spectrum (Figure 2d) suggests that the oligomer formed at pH 2 in the absence of salt is rich in α-helix and/or random coil structures. Their relative β-structure content appears to be higher than that of the monomeric protein at pH 4, which is evident from the relative peak intensities at 1619 and 1649 cm^{-1} (Figure 2c,d). The oligomer formed in the absence of NaCl shows a peak at ~1545 cm^{-1} in the amide II region as does the monomer at pH 4.

Panels e and f of Figure 2 show the FTIR spectra of oligomers formed at pH 2 in the presence of 120 and 200 mM NaCl, respectively. The FTIR spectra of the oligomers were recorded at a protein concentration of 500 μM, at which more than 98% of the protein molecules are present as oligomers as seen in size exclusion chromatography (data not shown). The FTIR spectra of oligomers formed in 120 and in 200 mM NaCl are drastically different (Figure 2e,f). In the amide I region, the oligomers formed in 120 mM NaCl show two peaks, at ~1620 and ~1650 cm^{-1}; in contrast, the oligomers formed in 200 mM NaCl show a single peak at ~1628 cm^{-1}. In the amide II region, the oligomers formed in 120 mM NaCl show a peak at ~1540 cm^{-1}, while those formed in 200 mM NaCl show a peak with a much lower relative intensity at ~1530 cm^{-1}. Each protein sample at pH 2 was equilibrated in 50 mM glycine buffer containing the desired amount of NaCl, for 1 h at 25 °C, prior to the spectroscopic characterization.

Probe Dependence of the Kinetics of Fibril Formation from the β-Rich Oligomer. The kinetics of fibril formation was monitored by measurement of the changes in ThT fluorescence, ellipticity at 216 nm (θ_{216}), mean R_H, and scattering intensity (SI). ThT fluorescence and θ_{216} are probes of β-sheet conformational changes during fibril formation, mean R_H probes the growth (elongation) of protein aggregates, and SI reports on both the size and the amount of protein aggregates. At each NaCl concentration and with each of the four probes, the kinetics was seen to be monophasic with no apparent lag phase. Each of the kinetic traces extrapolated, at time zero, to the signal obtained for the β-rich oligomer (data not shown). The experiments with each of the probes were highly reproducible, which is evident from the small errors seen in each of the measurements of the apparent rate constant (Figure 3a,b). In all these experiments, the protein remained fully soluble, and there were no insoluble aggregates that could have interfered with any of the spectroscopic measurements (data not shown).

Panels a and b of Figure 3 show the apparent rate constants of worm-like fibril formation by 25 μM protein at 50 °C and pH 2 in the presence of 120 and 200 mM NaCl, respectively. In 120 mM NaCl, the observed rate constant of the formation of worm-like amyloid fibrils is similar when monitored by the change in ThT fluorescence, θ_{216}, or SI (Figure 3a). The R_H-monitored kinetics is, however, seen to be ~2-fold faster than the kinetics monitored by the other three probes. In contrast, the ThT fluorescence- and θ_{216}-monitored kinetics are ~2-fold faster than the mean R_H-monitored kinetics for aggregation in 200 mM NaCl (Figure 3b). For aggregation in 120 mM NaCl, the SI-monitored kinetics

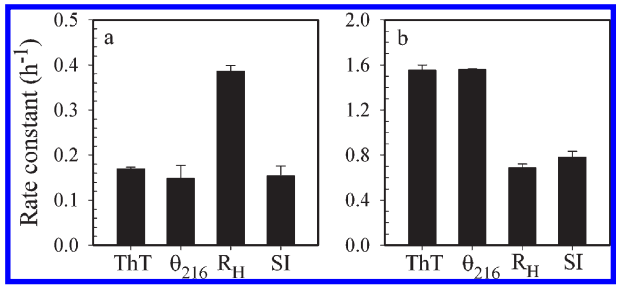

FIGURE 3: Probe dependence of the kinetics of amyloid fibril formation from the β-rich oligomer in 120 and 200 mM NaCl. Amyloid fibril formation by 25 μM protein was monitored using the mean hydrodynamic radius (R_H), ThT fluorescence (ThT), ellipticity at 216 nm (θ_{216}), and scattering intensity (SI) as probes. Apparent rate constants were determined from single-exponential fits of the kinetic traces of aggregation at 50 °C and pH 2 in the presence of 120 mM NaCl (a) and in the presence of 200 mM NaCl (b). The error bars represent the spreads in the values obtained from two independent experiments.

is slower than the kinetics monitored by mean R_H (Figure 3a). On the other hand, the SI-monitored kinetics is similar to the mean R_H-monitored kinetics for aggregation in 200 mM NaCl (Figure 3b).

Structures of Worm-like Amyloid Fibrils Formed at Low and High NaCl Concentrations. Figure 4a shows that the far-UV CD spectra of the worm-like fibrils formed in 120 and 200 mM NaCl are similar. The worm-like amyloid fibrils formed at both of these NaCl concentrations show the presence of β-rich structures, as evident from the minima at ~213−215 nm in the far-UV CD spectra. The R_H distributions shown in Figure 4b suggest that the worm-like amyloid fibrils formed in 200 mM NaCl are more heterogeneous than those formed in 120 mM NaCl, which is evident from the widths of the distributions. The mean values of R_H of the fibrils formed in 120 and 200 mM NaCl are ~37 and ~65 nm, respectively.

Panels c and d of Figure 4 show AFM images of the worm-like amyloid fibrils formed in 120 and 200 mM NaCl, respectively. At both of these salt concentrations, elongated, curly worm-like nanostructures were seen to form, similar to those that form in 150 mM NaCl at pH 2 and 60 °C (*37*). Their mean diameters, as determined from the *Z*-heights on AFM mica, are also similar (2.2 ± 0.4 nm in 120 mM NaCl and 1.9 ± 0.2 nm in 200 mM NaCl). Their mean lengths, determined from the AFM images, were found to be ~490 and ~540 nm in 120 and 200 mM NaCl, respectively. In both cases, many shorter and fewer longer fibrils were seen; fibril lengths were found to be exponentially distributed as expected (*45*) (data not shown). It should be noted that although the R_H distributions (Figure 4b) predict that the fibrils formed in 200 mM NaCl should be significantly longer than those formed in 120 mM NaCl, the direct measurements of the fibril lengths by AFM do not show a significant difference. It is unknown why the DLS measurement taken in bulk solution yields a larger difference in length than the AFM measurement taken on a mica surface. For fibrils formed in 200 mM NaCl, clumps of fibrils were seen in AFM images, and it is possible that longer fibrils have a greater tendency to be in clumps, where their lengths could not be measured. It is also possible that the longer fibrils stick less well to the surface of the mica.

Panels e and f of Figure 4 show the FTIR spectra of the worm-like amyloid fibrils formed at pH 2 in the presence of 120 and 200 mM NaCl, respectively. The FTIR spectra differ in both the amide I and amide II regions, which is also seen for the β-rich oligomers. In the amide I region, the worm-like fibrils formed in

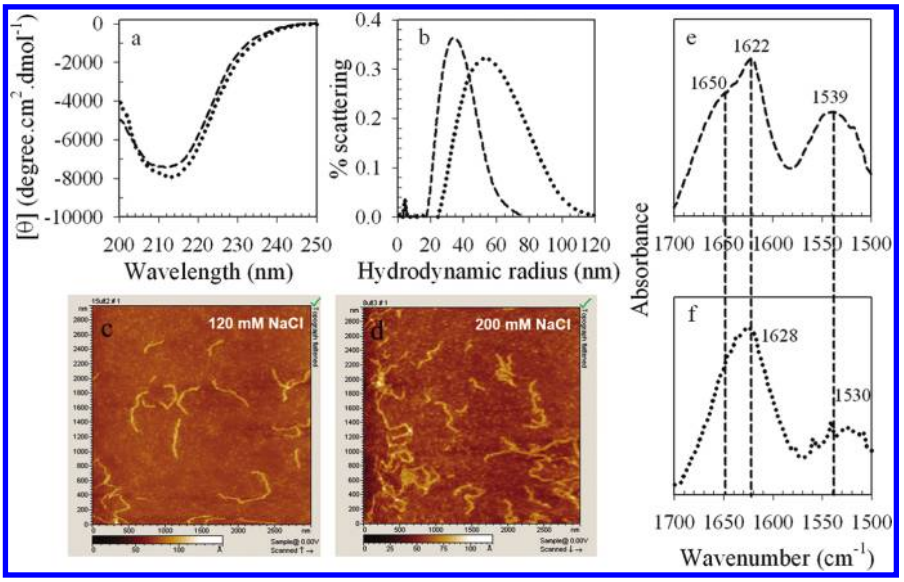

FIGURE 4: Structural characterization of the worm-like amyloid fibrils formed by 25 μM protein at 50 °C and pH 2 in 120 and 200 mM NaCl. Aggregation was conducted in the presence of 120 (---) and 200 mM NaCl (· · ·). The amyloid fibrils were characterized at a time corresponding to three time constants of the kinetics monitored by the slowest probe, at which time the aggregation process was virtually complete. (a) Far-UV CD spectra. (b) DLS distributions. (c) AFM images of worm-like amyloid fibrils formed in 120 mM NaCl. (d) AFM images of worm-like amyloid fibrils formed in 200 mM NaCl. (e) FTIR spectrum of worm-like amyloid fibrils formed in 120 mM NaCl. (f) FTIR spectrum of worm-like amyloid fibrils formed in 200 mM NaCl. For acquisition of the FTIR spectra, fibrils were concentrated to 500 μM (in 120 mM NaCl) or 200 μM (in 200 mM NaCl).

120 mM NaCl show two peaks, at ~1622 and ~1650 cm^{-1}; in contrast, the worm-like fibrils formed in 200 mM NaCl show a single peak at ~1628 cm^{-1}. In the amide II region, the worm-like fibrils formed in 120 mM NaCl show a peak at ~1539 cm^{-1}, while those formed in 200 mM NaCl show a peak of lower intensity at ~1530 cm^{-1}. Interestingly, the FTIR spectrum of the worm-like fibrils formed at each NaCl concentration is identical to that of the β-rich oligomers at the same NaCl concentration.

Effect of Different Anions on Fibril Growth. To understand the role of different anions, the effects of various salts, namely, Na_2SO_4, NaI, $NaNO_3$, and NaCl, on fibril growth were studied. The extent of fibril formation at different salt concentrations for each of these salts was determined by measurement of the amplitude of the change in ThT fluorescence intensity that occurs under each aggregation condition (*31*, *33*, *46*). The extent of fibril growth, as monitored by the amplitude of the change in the ThT fluorescence signal intensity, is seen to be dependent on the nature as well as on the concentration of the anion (Figure 5a). The efficacy of a salt in promoting aggregation was determined by determining that salt concentration at which the extent of fibril formation is half that seen at the saturating salt concentration. Hence, the order of the efficacies of the anions for promoting fibril growth was as follows: $SO_4^{2-} > I^- > NO_3^- > Cl^-$. Interestingly, the same order of efficacies is obtained when the minimum salt concentration required for maximum fibril formation is used as the criterion for efficacy, even though the dependence of the extent of fibril formation on salt concentration is different for each salt (Figure 5a). The minimum salt concentration at which fibril formation is maximum was found to be ~110, ~50, ~75, and ~10 mM for NaCl, NaI, $NaNO_3$, and Na_2SO_4, respectively.

Panels b–e of Figure 5 show the AFM images of amyloid fibrils formed after aggregation for 19 h at 50 °C, in the presence of 10 mM Na_2SO_4, 100 mM NaI, 100 mM $NaNO_3$, and 120 mM NaCl, respectively. Elongated and curly worm-like amyloid fibrils are seen to form in the presence of each of these salts. As evident from the AFM images, the fibrils vary in the amount formed and in their lengths, but they have similar heights (1.8 ± 0.2 nm in 10 mM Na_2SO_4, 2.0 ± 0.2 nm in 100 mM NaI, 2.1 ± 0.2 nm in 100 mM $NaNO_3$, and 2.2 ± 0.4 nm in 120 mM NaCl). It should be noted that the protein was seen to precipitate at higher salt concentrations under the aggregation conditions. The precipitation was seen at approximately ≥30−40 mM Na_2SO_4, ≥100 mM NaI, and ≥125 mM $NaNO_3$. No precipitation was seen at NaCl concentrations up to 200 mM.

DISCUSSION

The β-Rich Oligomers Formed at Low and High NaCl Concentrations Are Structurally Different. The β-rich oligomers formed in the absence of salt, in the presence of 120 mM NaCl, and in the presence of 200 mM NaCl differ significantly from one another in their sizes: the oligomer formed in 200 mM NaCl is larger than that formed in 120 mM NaCl (Figure 2b). The secondary structures are also found to be different (Figure 2).

The presence of peaks at 1620 and 1650 cm^{-1} in the FTIR spectra suggests that the oligomers formed in the absence of added salt as well as those formed in the presence of 120 mM NaCl possess both β-sheet and α-helical and/or random coil structures (Figure 2d,e). Interestingly, the relative amounts of these secondary structures differ in the oligomers formed under the two conditions: the oligomers formed in the absence of salt have similar α-helical and/or random coil structures and β-structures, while the oligomers formed in 120 mM NaCl have more β-structures than α-helical and/or random coil structures. The observation that the β-rich oligomers formed in 200 mM NaCl show a peak at 1628 cm^{-1} and do not show a peak at 1650 cm^{-1} (Figure 2f) suggests that it has more β-sheet and less of other secondary structure, if any. Furthermore, the observation that the position of the peak corresponding to β-sheet in the β-rich oligomers formed in 200 mM NaCl (1628 cm^{-1}) differs by 8 cm^{-1} from that in the case of oligomers formed in the absence

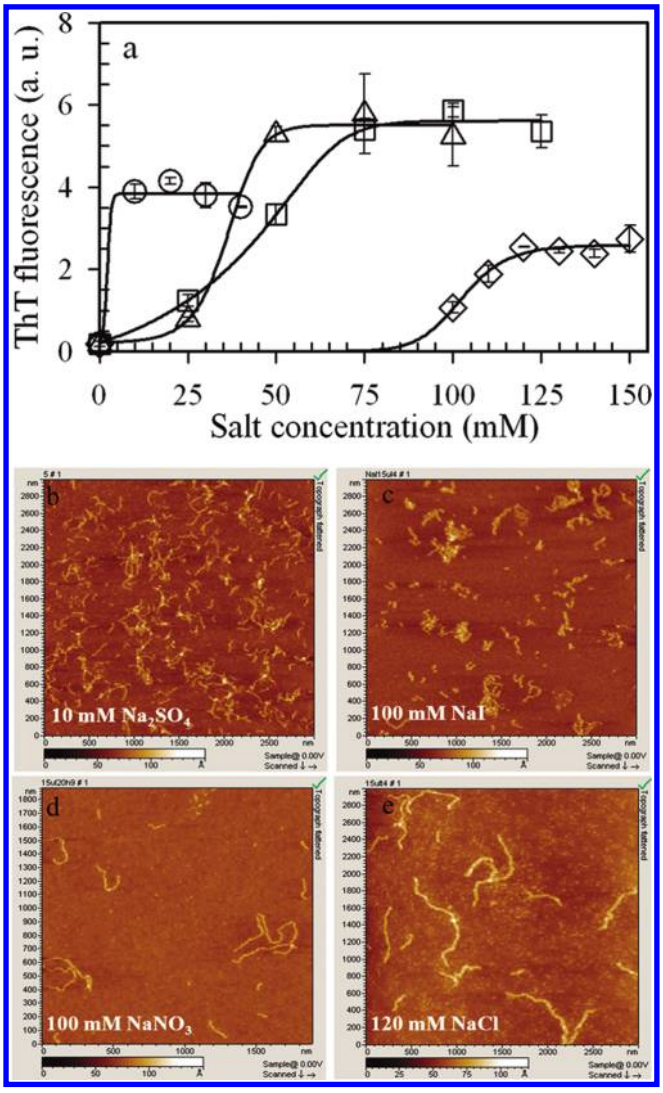

FIGURE 5: Effect of different anions on the growth of worm-like amyloid fibrils by 25 μM MoPrP at pH 2 and 50 °C. (a) Effect of different salts on amyloid fibril growth: Na_2SO_4 (○), NaI (△), $NaNO_3$ (□), and NaCl (◇). (b) AFM image of worm-like amyloid fibrils formed in 10 mM Na_2SO_4. (c) AFM image of worm-like amyloid fibrils formed in 100 mM NaI. (d) AFM image of worm-like amyloid fibrils formed in 100 mM $NaNO_3$. (e) AFM image of worm-like amyloid fibrils formed in 120 mM NaCl.

or presence of 120 mM NaCl (1620 cm^{-1}) suggests that the β-rich oligomers formed at low and high NaCl concentrations differ also in the internal structures of their β-sheets.

Mechanisms of Fibril Formation at Low and High NaCl Concentrations. The observation that worm-like fibril formation at low and high NaCl concentrations begins from β-rich oligomers of distinct structures and sizes suggests that the reaction must follow different mechanisms at the two NaCl concentrations. To delineate the steps involved in the two pathways, the probe dependence of the kinetics of worm-like fibril formation at low (120 mM) and high (200 mM) NaCl concentrations was monitored (Figure 3a,b).

The observation that in 120 mM NaCl, the ThT fluorescence- and θ_{216}-monitored kinetics are significantly slower than the mean R_H-monitored kinetics (Figure 3a) suggests that β-sheet conformational conversion follows aggregate elongation during the formation of worm-like fibrils in 120 mM NaCl (pathway I) (Figure 6a). Interestingly, the ThT fluorescence- and θ_{216}-monitored kinetics (Figure 3b) for aggregation in 200 mM NaCl (pathway II) (Figure 6b). This suggests that on this alternative pathway, the β-sheet conformational change precedes aggregate elongation. It appears that β-sheet conformational conversion at high NaCl concentration occurs in oligomeric intermediates, which further assemble into elongated fibrils. In a previous study of aggregation in 150 mM NaCl, it was shown that β-sheet conformational conversion occurs along with aggregate elongation (*37*). Hence, it appears that with an increase in NaCl concentration, the size and structure of the β-rich oligomers change in a gradual manner, and consequently, utilization of pathway II increases at the expense of utilization of pathway I.

In 120 mM NaCl, as in 150 mM NaCl (*37*), the observation that the SI-monitored kinetics is significantly slower than the kinetics monitored by the measurement of the mean R_H (Figure 3a) suggests that the elongated fibrils associate laterally in the final step to form mature worm-like fibrils. On the other hand, the SI- and mean R_H-monitored kinetics are very similar in 200 mM NaCl (Figure 3b). This suggests either that the elongated fibrils do not associate laterally on this pathway or that the lateral association occurs concurrently with the elongation. Since the heights of the worm-like amyloid fibrils formed in 120 and 200 mM NaCl are similar (see above), it appears that lateral association must occur concurrently with elongation at the higher NaCl concentration.

The Worm-like Fibrils Formed on the Alternative Pathways Differ in Their Structures. The alternative pathways commencing from structurally distinct β-rich oligomers lead to the formation of structurally different worm-like fibrils (Figure 6). The worm-like fibrils formed in 200 mM NaCl appear longer and more heterogeneous than those formed in 120 mM NaCl (Figure 4b) as suggested by the DLS distributions, although the length distributions made from the AFM images do not indicate that significantly longer fibrils are formed in 200 mM NaCl. The FTIR spectra of the worm-like fibrils formed in the two NaCl concentrations differ in the amide I as well as amide II regions (Figure 4e,f), suggesting that they differ also in their internal structures. The worm-like fibrils formed at both the NaCl concentrations have peaks in the 1613−1640 cm^{-1} region, suggesting that they are both rich in β-structures, but the positions of these peaks differ by ~6 cm^{-1}, which suggests that the fibrils differ in the internal structures of their β-sheets. Furthermore, the presence of a peak at 1650 cm^{-1} in the case of the worm-like fibrils formed in 120 mM NaCl (Figure 4e) suggests that they are not pure β-sheet structures but also possess other structures (α-helix and/or random coil). On the other hand, the worm-like fibrils formed in 200 mM NaCl do not show this peak at 1650 cm^{-1} (Figure 4f), suggesting that they consist of only β-structure and possess less of other structures, if any. The far-UV CD spectra and the heights in AFM images of the worm-like fibrils formed at low and high NaCl concentrations are, however, similar. It is also interesting to note that while the FTIR spectrum of the worm-like fibrils appears identical to that of the β-rich oligomer, at low or high salt concentration, the difference in secondary structure between the fibrils and their oligomeric precursors is, nevertheless, captured in the difference in the shapes of their CD spectra (Figures 2 and 4).

Salts Affect Fibril Formation of moPrP at Low pH by Preferential Anion Binding. Hydrophobic as well as electrostatic interactions are known to play important roles in the amyloid formation reactions of proteins and peptides. The extent of aggregation by a protein often shows a bell-shaped dependence on the concentration of salts (or organic cosolvents), which

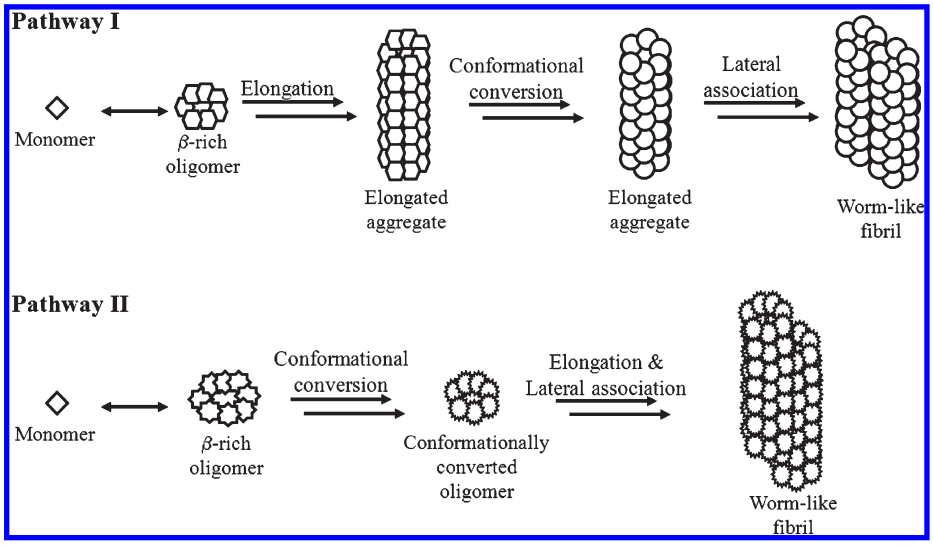

FIGURE 6: Pathways of worm-like fibril formation by the mouse prion protein. Pathway I is predominant at low salt concentration. The β-rich oligomer first grows in size to form elongated aggregates. The conformational conversion leading to the formation of ThT binding sites and an increase in the level of β-structure (as detected by CD) occurs in these elongated aggregates. Finally, these conformationally converted and elongated aggregates associate laterally to form mature worm-like amyloid fibrils. Pathway II is predominant at high salt concentration. The β-rich oligomer is structurally distinct from that formed at low salt concentration. These oligomers first change their conformation, leading to the formation of ThT binding sites and an increase in the level of β-structure. The conformationally converted oligomers then elongate and associate to form mature worm-like amyloid fibrils of distinct structure.

are known to affect hydrophobic and electrostatic interactions in a concentration-dependent manner (*31*, *46*). The bell-shaped dependence has suggested that the effect of salts or organic cosolvents on amyloid formation reactions depends on how these additives affect the balance between hydrophobic and electrostatic interactions (*31*, *46*).

There are several ways by which salts can modulate the hydrophobic and electrostatic interactions involved in the amyloid fibril formation reactions of proteins and peptides. Salts may exert their effects on these interactions by Debye−Huckel screening of the charges on protein molecules or by directly binding to these charges (*31*, *47*, *48*). They can also perturb water structure, thereby affecting the hydration of protein molecules (*49*−*51*).

In this study, it is seen that different anions exhibit different optimal concentrations at which they promote worm-like fibril formation by moPrP at low pH (Figure 5a). If the effect of the salt were predominantly through Debye−Huckel screening of protein charges, then the effect of salt would be expected to depend on the ionic strength regardless of the nature of the ions. Here, it is seen that while prion fibril growth is favored by 10 mM Na_2SO_4, the extent of fibril growth is far less at the equivalent ionic strength contributed by 30 mM NaCl (Figure 5a). This observation suggests that ionic strength alone cannot explain the observed behavior of these salts in affecting the growth of prion fibrils. If salts act by perturbing the water structure, then the effect is expected to follow the Hofmeister series, which for the anions used in this study, would be as follows: $SO_4^{2-} > Cl^- > NO_3^- > I^-$ (*49*−*51*). The ability of the different salts to promote worm-like fibril formation at low pH does not, however, follow the Hofmeister series; the order of anions in their ability to promote the reaction is as follows: $SO_4^{2-} > I^- > NO_3^- > Cl^-$ (Figure 5a). It therefore appears that perturbation of water structure cannot be the dominant factor in how salts affect fibril formation by moPrP.

Interestingly, the order of anions in their ability to promote worm-like fibril formation is consistent with the electroselectivity series of anions (*52*, *53*), suggesting that the preferential interaction (or binding) of anions with the positive charges on the protein modulates amyloid fibril formation. The anion binding-induced modulation is also evident from the sigmoidal dependence of the observed rate constant on NaCl concentration (Figure 1b). The very sharp sigmoidal dependence of the observed rate constant on NaCl concentration (Figure 1b) suggests that a large number of anions must bind to the protein to induce aggregation. The moPrP has a charge of +32 at pH 2, partly because 13 carboxyl groups of aspartate and glutamate side chains become protonated at this pH. It is possible that anion binding may occur at locations previously occupied by the negatively charged carboxyl groups at neutral pH.

In an anion binding model, the salt concentration at which the extent of fibril formation is half that seen at saturating salt concentrations is a measure of the binding constant for that salt. Hence, the order of the fibril-promoting efficacies of the anions [$SO_4^{2-} > I^- > NO_3^- > Cl^-$ (Figure 5a)] reflects the order of binding affinities of the anions to the protein. The dependence of the extent of fibril formation on salt concentration reflects the number of salt anions that bind to yield the maximum effect, and the cooperativity of anion binding is seen to be different for different anions. The observation that the final intensity of the ThT fluorescence signal, or the total ThT binding capacity, depends on the anion bound suggests that the structures of the fibrils formed depend on the nature and extent of anion binding.

Investigating the detailed thermodynamic linkage of anion binding to protein aggregation would be an intriguing prospect. There have been several detailed studies of the linkage of ion binding to protein folding reactions, and it has been seen that usually the binding of only very few ions appears to matter in the linkage (*54*−*57*). A detailed study of the linkage of anion binding to the aggregation of moPrP is a daunting prospect not only because the linkage must involve the binding of many anions (see above) but also because the size of the β-rich oligomer, from which worm-like fibrils form, appears to increase continuously in size with an increase in NaCl concentration from 120 to 200 mM (Figure 2b).

Recent studies have shown that anions can affect the fibril formation reactions of α-synuclein, histones, amyloid β, and β_2-microglobulin (*29*, *31*, *33*, *58*). Interestingly, in the case of α-synuclein, it was reported that the relative abilities of various anions in promoting fibril formation follow the Hofmeister series at salt concentrations of >10 mM, while electrostatic interactions dominate at lower salt concentrations (*29*). In the case of β_2-microglobulin, it was shown that preferential anion binding interactions play a predominant role in modulating amyloid formation (*31*), as is shown in this study for moPrP.

Hydrophobic interactions have to be considered in conjunction with electrostatic interactions, because a balance between the two interactions appears to be critical for amyloid formation or self-association (see above). The salt concentration used in this study is perhaps too low (<200 mM) to affect hydrophobic interaction significantly (*49*−*51*). This might suggest that hydrophobic interactions play a minor role in the worm-like fibril formation reaction of moPrP and that electrostatic interactions are the dominant determinants. However, while describing the effect of salts on protein conformation, these two interactions cannot be described in such a mutually exclusive manner. Hydrophobic interaction may become dominant in the self-assembly reaction only upon neutralization of the positive charges on the protein by anions, as seen in the case of oligomer formation by peptibody A (*59*). Anion binding will lead to neutralization of charge repulsion, allowing protein molecules to come together in closer proximity, which, in turn, allows hydrophobic interactions to facilitate further assembly. In this study, anion binding is shown to be an important factor in stabilizing oligomers of moPrP, as well as in determining the propensity of the oligomers to grow into worm-like fibrils.

ACKNOWLEDGMENT

We thank K. Gayathrie for preliminary experiments and members of our laboratory for discussions. The AFM images were recorded in the Central Imaging Facility of the National Centre for Biological Sciences (Bangalore, India).

REFERENCES

1. Prusiner, S. B. (1982) Novel proteinaceous infectious particles cause scrapie. *Science 216*, 136–144.
2. Caughey, B., Baron, G. S., Chesebro, B., and Jeffrey, M. (2009) Getting a grip on prions: Oligomers, amyloids, and pathological membrane interactions. *Annu. Rev. Biochem. 78*, 177–204.
3. Prusiner, S. B. (1998) Prions. *Proc. Natl. Acad. Sci. U.S.A. 95*, 13363–13383.
4. Collinge, J. (2001) Prion diseases of humans and animals: Their causes and molecular basis. *Annu. Rev. Neurosci. 24*, 519–550.
5. Aguzzi, A., and Polymenidou, M. (2004) Mammalian prion biology: One century of evolving concepts. *Cell 116*, 313–327.
6. Diringer, H., Gelderblom, H., Hilmert, H., Ozel, M., Edelbluth, C., and Kimberlin, R. H. (1983) Scrapie infectivity, fibrils and low molecular weight protein. *Nature 306*, 476–478.
7. Diener, T. O. (1987) PrP and the nature of the scrapie agent. *Cell 49*, 719–721.
8. Merz, P. A., Kascsak, R. J., Rubenstein, R., Carp, R. I., and Wisniewski, H. M. (1987) Antisera to scrapie-associated fibril protein and prion protein decorate scrapie-associated fibrils. *J. Virol. 61*, 42–49.
9. Caughey, B., and Chesebro, B. (1997) Prion protein and the transmissible spongiform encephalopathies. *Trends Cell Biol. 7*, 56–62.
10. Legname, G., Baskakov, I. V., Nguyen, H. O., Riesner, D., Cohen, F. E., DeArmond, S. J., and Prusiner, S. B. (2004) Synthetic mammalian prions. *Science 305*, 673–676.
11. Chien, P., Weissman, J. S., and DePace, A. H. (2004) Emerging principles of conformation-based prion inheritance. *Annu. Rev. Biochem. 73*, 617–656.
12. Wang, F., Wang, X., Yuan, C. G., and Ma, J. (2010) Generating a prion with bacterially expressed recombinant prion protein. *Science 327*, 1132–1135.
13. Parchi, P., Gambetti, P., Picardo, P., and Ghetti, B. (1998) Human prion diseases. In Progress in Pathology IV (Haddock, G. M., Ed.) pp 39−77, Churchill Livingstone, Edinburgh, U.K.
14. Millhauser, G. L. (2007) Copper and the prion protein: Methods, structures, function, and disease. *Annu. Rev. Phys. Chem. 58*, 299–320.
15. Pattison, I. H., and Jebbett, J. N. (1971) Histopathological similarities between scrapie and cuprizone toxicity in mice. *Nature 230*, 115–117.
16. Brown, D. R., Qin, K., Herms, J. W., Madlung, A., Manson, J., Strome, R., Fraser, P. E., Kruck, T., von Bohlen, A., Schulz-Schaeffer, W., Giese, A., Westaway, D., and Kretzschmar, H. (1997) The cellular prion protein binds copper in vivo. *Nature 390*, 684–687.
17. Hijazi, N., Shaked, Y., Rosenmann, H., Ben-Hur, T., and Gabizon, R. (2003) Copper binding to PrPC may inhibit prion disease propagation. *Brain Res. 993*, 192–200.
18. Sigurdsson, E. M., Brown, D. R., Alim, M. A., Scholtzova, H., Carp, R., Meeker, H. C., Prelli, F., Frangione, B., and Wisniewski, T. (2003) Copper chelation delays the onset of prion disease. *J. Biol. Chem. 278*, 46199–46202.
19. Colon, W., and Kelly, J. W. (1992) Partial denaturation of transthyretin is sufficient for amyloid fibril formation in vitro. *Biochemistry 31*, 8654–8660.
20. Booth, D. R., Sunde, M., Bellotti, V., Robinson, C. V., Hutchinson, W. L., Fraser, P. E., Hawkins, P. N., Dobson, C. M., Radford, S. E., Blake, C. C., and Pepys, M. B. (1997) Instability, unfolding and aggregation of human lysozyme variants underlying amyloid fibrillogenesis. *Nature 385*, 787–793.
21. Kelly, J. W. (1998) The alternative conformations of amyloidogenic proteins and their multi-step assembly pathways. *Curr. Opin. Struct. Biol. 8*, 101–106.
22. Uversky, V. N., and Fink, A. L. (2004) Conformational constraints for amyloid fibrillation: The importance of being unfolded. *Biochim. Biophys. Acta 1698*, 131–153.
23. McCutchen, S. L., Colon, W., and Kelly, J. W. (1993) Transthyretin mutation Leu-55-Pro significantly alters tetramer stability and increases amyloidogenicity. *Biochemistry 32*, 12119–12127.
24. Kumar, S., and Udgaonkar, J. B. (2009) Structurally distinct amyloid protofibrils form on separate pathways of aggregation of a small protein. *Biochemistry 48*, 6441–6449.
25. Kumar, S., and Udgaonkar, J. B. (2009) Conformational conversion may precede or follow aggregate elongation on alternative pathways of amyloid protofibril formation. *J. Mol. Biol. 385*, 1266–1276.
26. Uversky, V. N., Karnoup, A. S., Segel, D. J., Seshadri, S., Doniach, S., and Fink, A. L. (1998) Anion-induced folding of staphylococcal nuclease: Characterization of multiple equilibrium partially folded intermediates. *J. Mol. Biol. 278*, 879–894.
27. Uversky, V. N., Li, J., and Fink, A. L. (2001) Trimethylamine-N-oxide-induced folding of α-synuclein. *FEBS Lett. 509*, 31–35.
28. Uversky, V. N., Li, J., and Fink, A. L. (2001) Evidence for a partially folded intermediate in α-synuclein fibril formation. *J. Biol. Chem. 276*, 10737–10744.
29. Munishkina, L. A., Henriques, J., Uversky, V. N., and Fink, A. L. (2004) Role of protein-water interactions and electrostatics in α-synuclein fibril formation. *Biochemistry 43*, 3289–3300.
30. Yeh, V., Broering, J. M., Romanyuk, A., Chen, B., Chernoff, Y. O., and Bommarius, A. S. (2010) The Hofmeister effect on amyloid formation using yeast prion protein. *Protein Sci. 19*, 47–56.
31. Raman, B., Chatani, E., Kihara, M., Ban, T., Sakai, M., Hasegawa, K., Naiki, H., Rao, Ch. M., and Goto, Y. (2005) Critical balance of electrostatic and hydrophobic interactions is required for β2-microglobulin amyloid fibril growth and stability. *Biochemistry 44*, 1288–1299.
32. Pedersen, J. S., Flink, J. M., Dikov, D., and Otzen, D. E. (2006) Sulfates dramatically stabilize a salt-dependent type of glucagon fibrils. *Biophys. J. 90*, 4181–4194.
33. Klement, K., Wieligmann, K., Meinhardt, J., Hortschansky, P., Richter, W., and Fandrich, M. (2007) Effect of different salt ions on the propensity of aggregation and on the structure of Alzheimer's Aβ(1−40) amyloid fibrils. *J. Mol. Biol. 373*, 1321–1333.
34. Chien, P., DePace, A. H., Collins, S. R., and Weissman, J. S. (2003) Generation of prion transmission barriers by mutational control of amyloid conformations. *Nature 424*, 948–951.
35. Anderson, M., Bocharova, O. V., Makarava, N., Breydo, L., Salnikov, V. V., and Baskakov, I. V. (2006) Polymorphism and ultrastructural organization of prion protein amyloid fibrils: An insight from high resolution atomic force microscopy. *J. Mol. Biol. 358*, 580–596.

36. Makarava, N., and Baskakov, I. V. (2008) The same primary structure of the prion protein yields two distinct self-propagating states. *J. Biol. Chem. 283*, 15988–15996.
37. Jain, S., and Udgaonkar, J. B. (2008) Evidence for stepwise formation of amyloid fibrils by the mouse prion protein. *J. Mol. Biol. 382*, 1228–1241.
38. Bocharova, O. V., Breydo, L., Parfenov, A. S., Salnikov, V., and Baskakov, I. V. (2005) In vitro conversion of full-length mammalian prion protein produces amyloid form with physical properties of PrP^{Sc}. *J. Mol. Biol. 346*, 645–659.
39. Horcas, I., Fernández, R., Gómez-Rodríguez, J. M., Colchero, J., Gómez-Herrero, J., and Baro, A. M. (2007) WSXM: A software for scanning probe microscopy and a tool for nanotechnology. *Rev. Sci. Instrum. 78*, 013705.
40. Seshadri, S., Khurana, R., and Fink, A. L. (1999) Fourier transform infrared spectroscopy in analysis of protein deposits. *Methods Enzymol. 309*, 559–576.
41. Zandomeneghi, G., Krebs, M. R., McCammon, M. G., and Fandrich, M. (2004) FTIR reveals structural differences between native β-sheet proteins and amyloid fibrils. *Protein Sci. 13*, 3314–3321.
42. Susi, H. (1972) Infrared spectroscopy: Conformation. *Methods Enzymol. 26* (Part C), 455–472.
43. Riek, R., Hornemann, S., Wider, G., Billeter, M., Glockshuber, R., and Wüthrich, K. (1996) NMR structure of the mouse prion protein domain PrP(121−231). *Nature 382*, 180–182.
44. Donne, D. G., Viles, J. H., Groth, D., Mehlhorn, I., James, T. L., and Cohen, F. E.; et al. (1997) Structure of the recombinant full-length hamster prion protein PrP(29−231): The N terminus is highly flexible. *Proc. Natl. Acad. Sci. U.S.A. 94*, 13452–13457.
45. Howard, J. (2001) Polymerization of cytoskeletal filaments. In Mechanics of motor proteins and the cytoskeleton, pp 151−163, Sinauer Associates, Sunderland, MA.
46. Yamaguchi, K., Naiki, H., and Goto, Y. (2006) Mechanism by which the amyloid-like fibrils of a β2-microglobulin fragment are induced by fluorine-substituted alcohols. *J. Mol. Biol. 363*, 279–288.
47. Goto, Y., Calciano, L. J., and Fink, A. L. (1990) Acid-induced folding of proteins. *Proc. Natl. Acad. Sci. U.S.A. 87*, 573–577.
48. Goto, Y., Takahashi, N., and Fink, A. L. (1990) Mechanism of acid-induced folding of proteins. *Biochemistry 29*, 3480–3488.
49. Collins, K. D., and Washabaugh, M. W. (1985) The Hofmeister effect and the behaviour of water at interfaces. *Q. Rev. Biophys. 18*, 323–422.
50. Baldwin, R. L. (1996) How Hofmeister ion interactions affect protein stability. *Biophys. J. 71*, 2056–2063.
51. Zhang, Y., and Cremer, P. S. (2006) Interactions between macromolecules and ions: The Hofmeister series. *Curr. Opin. Chem. Biol. 10*, 658–663.
52. Gregor, H. P., Belle, J., and Marcus, R. A. (1955) Studies on ionexchange resins. XIII. Selectivity coefficients of quaternary base anion-exchange resins toward univalent anions. *J. Am. Chem. Soc. 77*, 2713–2719.
53. Gjerde, D. T., Schmuchler, G., and Fritz, J. S. (1980) Anion chromatography with low-conductivity eluents. *J. Chromatogr. 187*, 35–45.
54. Pace, C. N., and Grimsley, G. R. (1988) Ribonuclease T1 is stabilized by cation and anion binding. *Biochemistry 27*, 3242–3246.
55. García-Moreno, B. (1994) Estimating binding constants for site-specific interactions between monovalent ions and proteins. *Methods Enzymol. 240*, 645–667.
56. McCrary, B. S., Bedell, J., Edmondson, S. P., and Shriver, J. W. (1998) Linkage of protonation and anion binding to the folding of Sac7d. *J. Mol. Biol. 276*, 203–224.
57. Rami, B. R., and Udgaonkar, J. B. (2001) pH-jump-induced folding and unfolding studies of barstar: Evidence for multiple folding and unfolding pathways. *Biochemistry 40*, 15267–15279.
58. Munishkina, L. A., Fink, A. L., and Uversky, V. N. (2004) Conformational prerequisites for formation of amyloid fibrils from histones. *J. Mol. Biol. 342*, 1305–1324.
59. Gokarn, Y. R., Fesinmeyer, R. M., Saluja, A., Cao, S., Dankberg, J., Goetze, A., Remmele, R. L., Jr., Narhi, L. O., and Brems, D. N. (2009) Ion-specific modulation of protein interactions: Anion-induced, reversible oligomerization of a fusion protein. *Protein Sci. 18*, 169–179.